

UNIVERSITY OF OSLO
Department of
Geosciences

**Is there a positive
feedback between
Arctic stratus and
Arctic sea ice
changes?
Master thesis**

Master thesis in
Geosciences
Meteorology and
oceanography

Mari Fenn
Kristiansen

1st June 2015



*Rows and flows of angel hair
and ice cream castles in the air
and feather canyons
everywhere,
I've looked at clouds that way.*

JONI MITCHELL

Abstract

This will be my abstract.

Write it later....

No more than a page and should contain:

- main findings - how it compares to others - a conclusion?

Acknowledgements

First of all I want to thank my main supervisor Jón Egill Kristjánsson for an interesting project and for the opportunity to come and work at NCAR for a couple of weeks. I also want to thank my other supervisor Kari Alterskjaer for her "poking" and setting deadlines and pushing me for the past six months. I greatly appreciate their guidance and criticism throughout this project, and the doors that were always safe to knock on.

Thank you so much to Anne Claire Fullioux for helping me with setting up and getting started with WRF, and to both her and Kjell Andresen for help with technical problems during my work with this thesis. Thanks should also be given to Kjetil Schanke Aas for always taking time to answer any stupid WRF-related questions I might have had.

Thanks also to Gregory Thompson whom Jón Egill and I met with in Boulder, for meeting with us and answering all my e-mails about running the new aerosol-aware microphysics scheme in WRF.

These past two years have been very enjoyable in all their stress thanks to Marta and Helle especially, for all their positiveness.

Last, but not least, I would like to thank Henrik Andersen Sveinsson, for great technical help and moral support. @++

Contents

1	Introduction	9
1.1	Main goal	9
1.2	My contribution	10
1.3	Area description	10
1.4	Background	11
1.5	Structure of the thesis	12
2	Theory of Clouds and Radiation	13
2.1	Cloud effects on radiation	13
2.1.1	The Cloud – a gray body	13
2.1.2	Cloud optical depth	14
2.1.3	Cloud albedo	15
2.1.4	Cloud droplet effective radius	15
2.1.5	Liquid water content and path	16
2.1.6	Ice water path	18
2.2	Aerosols and clouds	18
2.2.1	The first indirect effect	19
2.2.2	The second indirect effect	20
2.3	Arctic stratus	20
3	Model and methods	23
3.1	Description of the WRF-ARW Modeling System	23
3.1.1	The vertical coordinate	24
3.1.2	Staggered grid	25
3.2	Model setup	26
3.2.1	Choices of physics in the model	27
3.3	Model runs	29
3.3.1	Manipulation of input files	30
3.4	Input data	30
3.5	Processing of the results	31

4 Results and discussion	33
4.1 Reference figures from the control run	33
4.2 Removed sea ice	33
4.2.1 Day 2	33
4.2.2 Day 5	37
4.3 Increased aerosol concentration	37
4.3.1 Day2	37
4.3.2 Day 5	38
4.4 The control run figures	41
5 Summary and Conclusions	47

Chapter 1

Introduction

Low clouds have a net warming effect in the Arctic [Intrieri *et al.*, 2002b], as opposed to the well known net cooling effect they have at lower latitudes. Low layered clouds (stratus) also dominate the Arctic cloud cover. The Arctic climate changes have been greater than the global mean and have become known by the term "Arctic amplification" [Graversen *et al.*, 2008]. Therefore the climate effect of low clouds in the Arctic is an interesting topic to study.

Decreasing sea ice extent could lead to an increase in the aerosol number concentrations in the area where ice has retreated. The open sea surface it self would lead to an increase in release of sea salt and DMS (dimethyl sulfide) to the lower atmosphere. The lack of sea ice would also increase the likelihood that the sea could be used for shipping, which would pollute the area.

The enhancement of evaporation from diminishing sea ice and the increase in aerosol number concentration from open water and shipping could lead to denser and longer-lived low clouds in the area of sea ice retreat. A followup question to that is if these clouds would then have a slightly different radiative effect, and by that influence the further retreat of sea ice.

This warming is due the emission of longwave radiation that reaches the surface. At lower latitudes the clouds ability to reflect shortwave radiation would have a large enough cooling effect for the longwave emissions to be overpowered. In the Arctic the polar night in winter and high zenith angles in summer reduce the available shortwave radiation to reflect drastically, and the emission of longwave radiation outweighs the cooling effect by reflecting the shortwave radiation @[\(cite Intrieri, the right one\)](#)

1.1 Main goal

According to the IPCC report by Boucher *et al.* [2013] the study by Eastman & Warren [2010a] using visual cloud reports from the Arctic, with sur-

face and satellite observations, and the studies by Kay & Gettelman [2009] and Palm *et al.* [2010] using lidar and radar observations have confirmed that the low-cloud amount over the Arctic oceans varies inversely with sea ice amount. This means that there is an increase in cloud amount when there is less sea ice. Now what we want to know is if these clouds are also denser and more persistent, and could lead to an enhanced warming and reduced sea ice amount, a positive feedback.

With this thesis I try to find if a decrease in Arctic sea ice lead to denser and more persistent clouds. It has been suggested that the decline in sea ice extent would allow for more pollution in the Arctic, as a consequence of more open water and ship traffic. The effect of increase in aerosol concentrations from shipping and open water, and the effect of enhanced evaporation from open water are studied separately and combined. With the main goal to find if this would lead to changes in clouds that could enhance downwelling long wave radiation and decrease upwelling short wave radiation, both of which have warming effects.

1.2 My contribution

The findings in my thesis have been achieved with some of the most recently developed code (by Greg Thompson [Thompson & Eidhammer, 2014]) for cloud micro physics and aerosols and their effects on radiation, in modeling. The results build further on the work of other researchers @name-some-and-cite and may raise some questions for further research within the field.

1.3 Area description

The area of the study in this thesis is in the Arctic, north of the United States of America and north-west of Canada. The study area covers the Beaufort Sea and small parts of Alaska and Canada, and can be seen in figure 1.1.

There are a few reasons for choosing this as the study area. First it is in the Arctic, and sea ice is present there in autumn, even in 2012 when there was record low sea ice extent. Also it has been exposed to field campaigns: Surface Heat Budget of the Arctic Ocean (SHEBA) [Uttal *et al.*, 2002], First International Satellite Cloud Climatology Project Regional Experiment Arctic cloud Experiment (FIRE ACE) [Curry *et al.*, 2000], Mixed-Phase Arctic Cloud Experiment (M-PACE) [Verlinde *et al.*, 2007] and more. Therefore there are many studies on Arctic clouds that include this study area and data from some of the mentioned field campaigns. This provides parts of the science basis for my study and selection of literature and studies for comparison and questions. Quite a few studies are based on satellite data

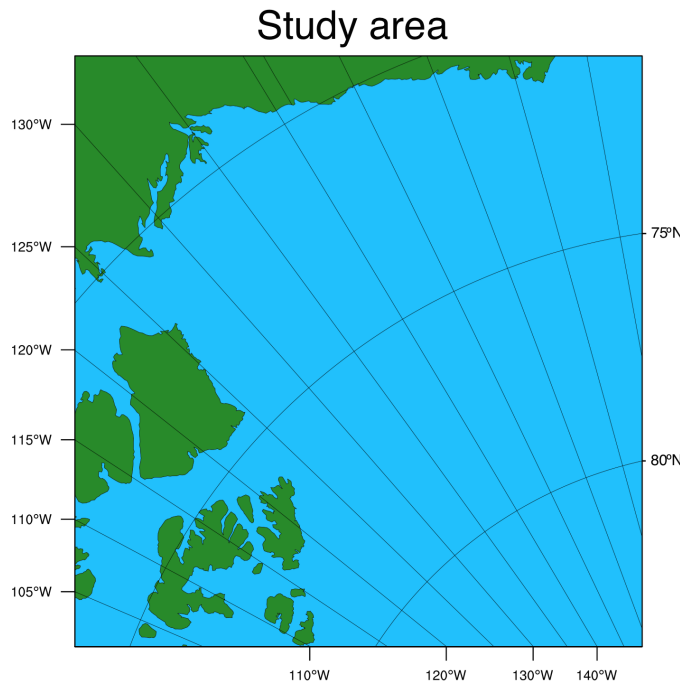


Figure 1.1: An overview of the study area. The bottom right corner is the northernmost point and the y-axes show longitude and latitude to the left and right, respectively.

analysis and some of them are presented in the next chapter as background and motivation for my thesis.

1.4 Background

In this chapter I shall present some recent literature on the subject, that forms a basis for the study presented in this thesis.

A study by Schweiger *et al.* [2008] investigated the connection between sea ice variability and cloud cover over the Arctic seas during autumn. They analysed the ERA-40 re-analysis products and some satellite data sets. They found that sea ice retreat was linked to a decrease in low-level (surface to ~ 1.9 km) cloud amount and an increase in mid-level (~ 1.9 to 6.1 km) clouds. They state that the decrease in static stability and deepening of the atmospheric boundary layer, following ice retreat, contribute to the rise in cloud level.

The study by Vavrus *et al.* [2010] investigated the behaviour of clouds, during intervals of rapid sea ice loss in the Arctic in the 21st century. The study was done by use of the Community Climate System Model (CCSM3). Their results support that cloud changes appear to accelerate rapid loss of

sea ice in autumn, and possibly in winter. They also conclude that "the trends in total cloudiness during rapid ice loss events are explained almost entirely by low-level clouds" and that "a positive feedback from primarily low cloud changes amid a warming climate".

Kay & Gettelman [2009] combined satellite data and complementary data sets to study the Arctic cloud and atmospheric structure during summer and early Autumn over the years 2006-2008. This covers the at the time record low sea ice extent from 2007. In contrast to the study by Schweiger *et al.* [2008] they found more low-level cloud. There are reasons to believe that the observations used in their study are more accurate than the re-analysis used in Schweiger *et al.* [2008].

Eastman & Warren [2010b] analysed visual cloud reports from the Arctic for year-to-year variations and found that following a low-ice September there would be enhanced low cloud cover.

The study by Palm *et al.* [2010] using satellite and lidar data and found that areas of open water were associated with greater polar cloud fraction.

A common uncertainty and missing link in a few of these studies is that they did not look at liquid water content, effective radii and other parameters affecting the radiative properties of the clouds. In this study, that is what I want to look in to, how these properties are influenced by the changing sea ice, and if the clouds enhance the sea ice melt.

1.5 Structure of the thesis

In the following chapter, Chapter 2, the most important theory needed to understand some of the processes in clouds and their possible effect on the sea ice is presented. Chapter 3 is where I explain which model and tools and I have used and how I have worked with them to get the results presented and discussed in chapter 4. A summary of main findings and conclusions are presented in the last chapter 5.

Chapter 2

Theory of Clouds and Radiation

In this thesis the term shortwave (SW) refers to the wavelength band that carries most of the energy associated with solar radiation, including the visible spectrum and the shorter waves in the near infrared ($\lambda < 4\mu m$ [Wallace & Hobbs, 2006]). Longwave (LW) refers to wavelengths emitted by the earth-atmosphere system (terrestrial radiation) including the longer waves in the near infra red and wavelengths in the infrared spectrum ($\lambda > 4\mu m$ [Wallace & Hobbs, 2006]).

In this chapter how cloud properties can influence radiation is presented, followed by a section on cloud effects on aerosols. Lastly a brief overview of clouds in the Arctic, with focus on stratus, is presented.

2.1 Cloud effects on radiation

The cloud microphysical properties that determine the cloud radiative properties include: the amount of condensed water, the size and shape of the cloud particles, and if the particles are liquid or ice [Curry *et al.*, 1996].

2.1.1 The Cloud – a gray body

Stefan–Boltzmanns law states that the flux density emitted by a blackbody is proportional to the fourth power of the absolute temperature [Liou, 2002].

$$F = \epsilon_\lambda \sigma T^4 \quad (2.1)$$

where $\epsilon_\lambda = 1$ is the emissivity for a blackbody at wavelength λ . F ($W m^{-2}$) is the flux density emitted by the body, and $\sigma = 5.67 \cdot 10^{-8} J m^{-2} sec^{-1} K^{-4}$ is the Stefan–Boltzmann constant. A blackbody both absorbs and emits at maximum, and the ratio of absorption and emission to the maximum is given by the absorptivity, α_λ , and the emissivity, ϵ_λ , for wavelength λ . Kirchoff's

law states that the absorptivity and emissivity for a medium are equal for each wavelength in the longer wavelength spectra: $\alpha_\lambda = \epsilon_\lambda$ [Liou, 2002]. Kirchoff's law is only applicable for LW radiation at local thermodynamic equilibrium in the lower 60-70 km of the atmosphere. Since this study focuses on the lowest 2 km of the troposphere, the law is applicable.

A cloud can be defined as a gray body, which means that α_λ and ϵ_λ are not maximum, $\alpha_\lambda = \epsilon_\lambda < 1$ [Liou, 2002].

The cloud LW emissivity, ϵ_{lw} , is a measure of the emittance of LW radiation by the cloud. From Stefan-Boltzmann's law, equation 2.1, the flux density emitted by a body depends on the body's temperature and its emissivity. The cloud longwave emissivity is given by

$$\epsilon_{lw} = 1 - \exp(-\beta\tau_{lw}) \quad (2.2)$$

where β is the diffusivity factor, having an approximate value of 1.66, and τ_{lw} is the cloud optical depth for longer wavelengths. Equation 2.1 shows that if one assumes constant cloud temperature, the flux density emitted by the cloud increases with increasing ϵ_{lw} , which increases with increasing τ_{lw} . Name some typical values, and calculate F?@

2.1.2 Cloud optical depth

Cloud optical depth (or cloud optical thickness) in the SW, τ_{sw} , is a measure of the cumulative depletion that a beam of radiation directed straight downward (zenith angle $\theta = 0$) would experience in passing through a defined cloud layer. Of the incident SW radiation on a cloud with optical depth τ_{sw} , a fraction $e^{-\tau_{sw}}$ is not scattered and is defined as the transmissivity of the cloud – the radiation that is not absorbed or scattered in passing through the cloud [Wallace & Hobbs, 2006]. The remaining $1 - e^{\tau_{sw}}$ has been scattered on or more times in passing through the cloud layer. The cloud optical depth is given by [Twomey, 1977]

$$\tau_{sw} = \int_0^h k_E dz = \pi \int_0^h \int_0^\infty r^2 Q_E(r/\lambda) n(r, z) dr dz \quad (2.3)$$

at height z above cloud base for a cloud of depth h , containing $n(r)dr$ drops with radius in the interval $(r, r+dr)$ per cubic centimeter (cm^{-3}). $Q_E(r/\lambda)$ is the extinction efficiency and k_E is the extinction coefficient [Twomey, 1977]. The extinction efficiency is a measure of how well a particle removes the incident radiation, either by scattering or absorption. In the visible, for $\lambda \ll r$, $Q_E \approx 2$ is a good approximation [?], and we get the simpler expression

$$\tau_{sw} = 2\pi N r_e^2 h \quad (2.4)$$

where it is assumed that the cloud droplet radius can be approximated by the effective radius, r_e . For longer wavelengths, the extinction efficiency can be assumed $Q_E \approx 4$ (@check this!) , and thereby gives a simpler expression for the cloud optical depth in the LW

$$\tau_{lw} = 4\pi N r_e^2 h \quad (2.5)$$

Knowing equation 2.2 it is clear that an increase in τ_{lw} will decrease the second term in equation 2.2, and hence increase ϵ_{lw} , which following Stefan-Boltzmann's law, equation 2.1, means that the flux density emitted by the cloud is increased, provided the cloud temperature is kept constant.

2.1.3 Cloud albedo

In section 2.1.2 it was stated that the incident SW radiation on a cloud layer is either transmitted or scattered. The scattered radiation is scattered by single droplets, and the single-scattering albedo, $\bar{\omega}$, is the fraction of energy that is not absorbed in a single-scattering event, but scattered. $\bar{\omega}$ can to a good approximation be assumed equal to 1. Which means that the absorption of SW is negligible for cloud water, which supports that the SW radiation is either transmitted or scattered. When the single-scattering albedo is taken to unity, the albedo (or reflectance) of a cloud layer is given by [?]

$$A = \frac{(1-g)\tau_{sw}}{1 + (1-g)\tau_{sw}} = \frac{1-g}{\frac{1}{\tau_{sw}} + (1-g)} \quad (2.6)$$

The cloud albedo, A , is then a function of the SW optical depth of a cloud, τ_{sw} , and the asymmetry factor g . The asymmetry factor gives the direction of scattered radiation by the cloud, and is given by $g = \cos \theta$ where θ is the scattering angle. g is a power-averaged value of the cosine of the scattering angle [Twomey, 1974]. $g = 1$ indicates pure forward scattering and $g = -1$ indicates pure back-scattering. According to Twomey, $g = 0.8$ or 0.9 for warm clouds, which means that most of the scattered energy is scattered forward.

2.1.4 Cloud droplet effective radius

The cloud droplet effective radius determines important radiative properties of a cloud, cloud albedo (A) and cloud emissivity (ϵ) [Hansen & Travis, 1974], and is therefore of particular interest.

The cloud droplet effective radius is a mean of the size distribution of cloud droplets, weighted by the droplet cross section. The effective radius, r_e , may be written

$$r_e = \frac{\int r^3 n(r) dr}{\int r^2 n(r) dr} \quad (2.7)$$

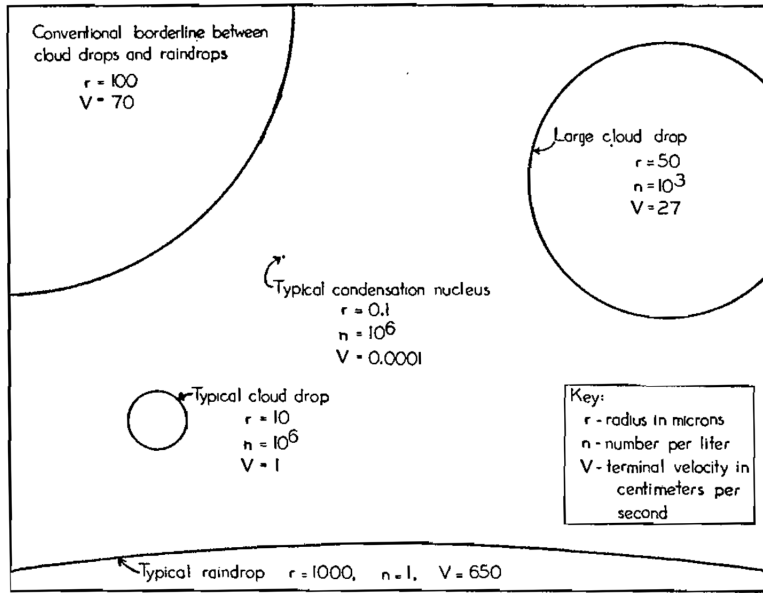


Figure 2.1: Typical sizes of cloud condensation nuclei (CCN), cloud droplet, large cloud droplet, borderline between cloud droplet and raindrop and typical size of raindrop. From [McDonald, 1958].

It can be seen from equations 2.4 and 2.5 that a decrease in r_e , when N and h is kept constant decreases the optical depth of the cloud in both SW, τ_{sw} and LW, τ_{lw} . Whereas an increase in r_e increases the cloud optical depths. It has already been established from equations 2.6 and 2.2 that a(n) decrease (increase) in the cloud optical depth leads to a(n) deacrease (increase) in the cloud albedo A and emissivity ϵ_{lw} .

The effective radius is typically on the order of a few micro meters μm . Typical size of a cloud droplet is depicted in figure 2.1. The figure also includes typical sizes of cloud condensation nuclei (CCN), large droplet, borderline between cloud droplet and raindrop and typical size of a raindrop.

2.1.5 Liquid water content and path

The amount of condensed water can be expressed by the liquid water content (LWC) in the cloud, often presented with units g m^{-3} and is proportional to the cloud droplet number concentration (CDNC), and cloud particle size. From Rogers & Yau [1989] we can express the number of droplets with radius r by

$$N = \int n(r)dr \quad (2.8)$$

where N is the CDNC (cm^{-3}), and $n(r)$ is the number of droplets with radius r . If we approximate the radius to be the effective radius, r_e (μm),

the LWC can be written (@@ should this be r_e or \bar{r} ??

$$\text{LWC} = \int \rho_l \frac{4}{3} \pi r^3 n(r) dr \quad (2.9)$$

$$= \frac{4}{3} \pi \rho_l \int r^3 n(r) dr \quad (2.10)$$

$$= \frac{4}{3} \pi \rho_l r_e^3 \int n(r) dr \quad (2.11)$$

$$= \frac{4}{3} \pi \rho_l r_e^3 N \quad (2.12)$$

where the last equation shows the proportionality of LWC to the cloud droplet number concentration N , and to r_e . ρ_l is the density of liquid water.

Another common measure of condensed water is the liquid water path (LWP). If the LWC is integrated over a column, from the base to the top, it gives the LWP of that column.

$$\text{LWP} = \int_{\text{base}}^{\text{top}} \text{LWC} dz \quad (2.13)$$

The LWP is the column of liquid water in a cloud and is usually expressed in g m⁻².

What effect a change in LWP has on incoming and outgoing radiation can be seen when the cloud optical depth is expressed as a function of LWP. Recall the cloud optical depth for SW radiation from equation 2.4 and rewrite it to get the CDNC (N) on the left side

$$N = \frac{\tau_{sw}}{2\pi r_e^2 h} \quad (2.14)$$

If the equation for LWC, equation 2.12, is also rewritten to get N on the left side, like so

$$N = \frac{3\text{LWC}}{4\pi \rho_l r_e^3} \quad (2.15)$$

the cloud optical depth in the visible (τ_{sw}) can be written as a function of LWP and r_e :

$$\frac{\tau_{sw}}{2\pi r_e^2 h} = \frac{3\text{LWC}}{4\pi \rho_l r_e^3} \quad (2.16)$$

$$\tau_{sw} = \frac{2\pi r_e^2 h 3\text{LWC}}{4\pi \rho_l r_e^3} \quad (2.17)$$

$$\tau_{sw} = \frac{3\text{LWC}h}{2\rho_l r_e} \quad (2.18)$$

$$\tau_{sw} = \frac{3\text{LWP}}{2\rho_l r_e} \quad (2.19)$$

Where (LWC $h \approx \text{LWP}$) It is now clear that, if the droplet size is constant, an increase in the LWP increases the optical depth of a cloud in the SW spectra, τ_{sw} . An increase in τ_{sw} would make the denominator in equation 2.6 for the cloud albedo, A , smaller and thereby increase the cloud albedo. An increase in A also means a reduction in SW radiation reaching the surface. In that way, an increase in LWP would have a cooling effect. But, we also need to consider the LW radiation.

Equation 2.2 shows a dependence of the cloud optical depth in the LW spectra, which is given by

$$\tau_{lw} = \frac{3\text{LWP}}{4\rho_l r_e} \quad (2.20)$$

which is simply half of τ_{sw} . The difference in cloud optical depth for SW and LW is due to the difference in the extinction efficiency, $Q_E(r/\lambda)$, which is dependent on the wavelength, ratio r/λ . Since longer waves are closer to the size of r than shorter waves, Q_E is smaller for longer waves.

2.1.6 Ice water path

The cloud may also consist of ice, not just liquid water, and for that

2.2 Aerosols and clouds

Aerosols have a direct effect on the climate by scattering and absorbing SW radiation, and scattering, absorbing and emitting LW radiation. A small subset of the atmospheric aerosols also serve as particles which water vapor can condense on to form droplets [Wallace & Hobbs, 2006]. Aerosols upon which water vapor can condense are called cloud condensation nuclei (CCN). Typical size for CCN is shown in figure 2.1. For low temperatures (~ -20 to -5degC) [Wallace & Hobbs, 2006], a few aerosols act as ice nuclei (IN) which if present allow for cloud ice to form. With IN cloud ice can form through heterogeneous freezing, contact nucleation and deposition [Wallace & Hobbs, 2006]. Heterogeneous freezing is when a droplet already contains a freezing nucleus and is brought to lower temperatures so that the already condensed water on the particle freezes. Contact nucleation is when a supercooled droplet (droplet with temperature below 0degC) is hit by a suitable ice nucleus, and deposition is when water vapor freezes directly on the nucleus.

@Mention which aerosols act as what, and how many of the total aerosol burden!

Through clouds the aerosols that act as CCN or IN also have an indirect effect. The amount of CCN and IN available affect the properties of the clouds. There are two known indirect effects that aerosols have on climate, through clouds.

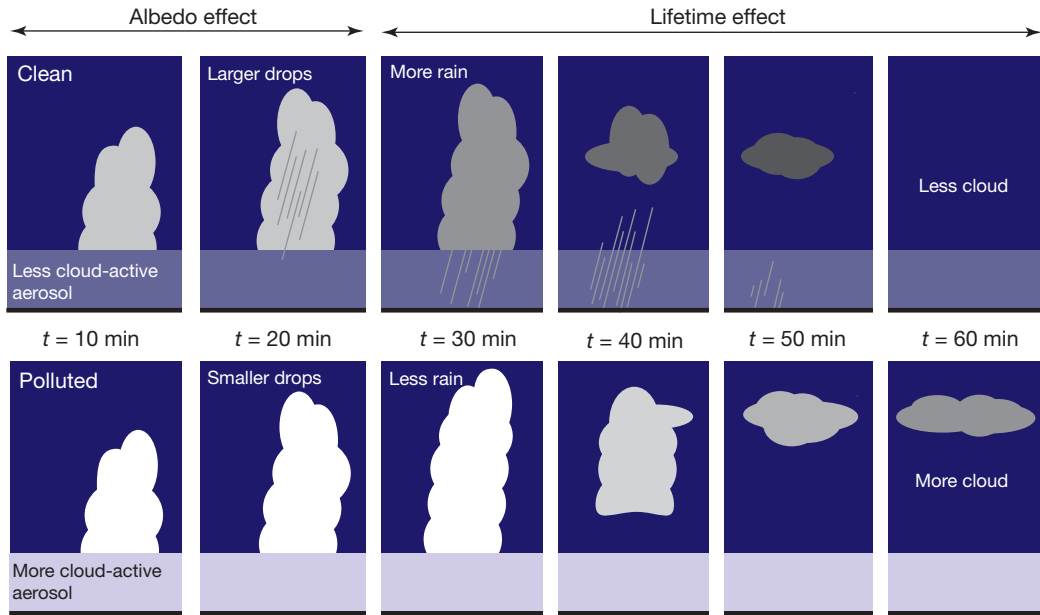


Figure 2.2: Figure showing the first indirect effect (albedo effect) to the left and the second indirect effect (lifetime effect) to the right. The figure includes a time axis to show the time scale of a precipitation process. The upper and lower panel show the clean and polluted case respectively. The figure is taken from Stevens & Feingold [2009].

2.2.1 The first indirect effect

The first indirect effect was proposed by Twomey [1974] and is often referred to as the Twomey effect. It describes the enhancement of cloud albedo as a consequence of an increase in aerosol content and thereby available CCN.

If there are few CCN in an area, a cloud formed there would be a clean cloud with few, but large droplets and therefore have a low albedo. If the area had high aerosol concentration, the cloud would be polluted and have more numerous but smaller droplet, provided the LWP is the same, which means it would have a higher optical depth in the SW according to equation 2.19, which through equation 2.6 gives a higher albedo.

Equation 2.4 shows that, if the effective radius is kept constant, the cloud optical depth will change with changes in CDNC (N in the equation). The CDNC is affected by the number of available CCN, and as the aerosol number concentration changes so will the number of CCN, and hence the CDNC and optical depth. Furthermore if a cloud has many small droplets, the cloud optical depth will be higher. Whereas fewer cloud droplets will yield a lower optical depth, provided r_e is kept constant, resulting in more SW radiation reaching the ground.

The increase in cloud albedo due to pollution is shown in the left-most 4 figures in figure 2.2. The figure shows that with more CCN available, in a polluted environment, the cloud or cloud layer, appears brigther than when the air is clean (fewer available CCN).

2.2.2 The second indirect effect

The second indirect effect was proposed by Albrecht [1989], and is also known as the lifetime effect.

The second indirect effect suggests more numerous but smaller droplets reduce the precipitation efficiency and by that enhances the cloud lifetime and hence the cloud reflectivity [Albrecht, 1989]. The effect is depicted in figure 2.2 as the lifetime effect, where it is shown that in the lower panel, the polluted case, the cloud does not precipitate and is therefore still present after an hour, where as the cloud in the upper panel, the clean case, is gone due precipitation.

Figure 2.1 shows that droplets have to grow to a size of typically $1000\mu\text{m}$ for precipitation to form. A rain drop is formed when smaller droplets collide and coalesce into a larger droplet, which also fails to collect smaller droplets until it is large enough to fall out of a cloud as precipitation. The second indirect effect suggests that an increase in aerosol burden leads to the water vapor being spread over a higher number of droplets, giving them a smaller effective radius which will prohibit them from growing to a raindrop. The hypothesis is that if the cloud does not precipitate, it will grow denser and live longer since the cloud water is not removed by precipitation. According to Lohmann & Feichter [2005] this effect had been estimated to be of the same order as the first indirect effect. It has since been shown that the effect is in fact small globally averaged [Stevens & Feingold, 2009]. Stevens & Feingold [2009] state that in the cases where an increased aerosol burden prohibits precipitation, the cloud can be entrained by dryer air which leads to evaporation of the cloud droplets, and the cloud ceases to exist. On the other hand, an increase in aerosol burden in deep precipitating clouds may lead to more, not less precipitation [Stevens & Seifert, 2008].

2.3 Arctic stratus

Clouds in the Arctic differ from clouds elsewhere in that they have a net warming effect, as opposed to the global mean net cooling effect [Shupe & Intrieri, 2004]. Winter in the Arctic (polar night) is completely dark and free of incoming SW radiation. The Arctic summer on the other hand has sunlight 24/7. The amount of solar radiation reaching the surface is limited by the optical depth of the atmosphere it passes through. The normal optical depth is a measure of the cumulative depletion of a radiation beam directed

straight downward (zenith angle $\theta = 0$) from the top of the atmosphere to a level z , defined by [Wallace & Hobbs, 2006]

$$\tau_{norm} = \int_z^\infty k_\lambda \rho_a R dz \quad (2.21)$$

where k_λ is the mass absorption coefficient, ρ_a is the density of air and R is the mass of absorbing gas per unit mass of air. The undepleted fraction of the radiation is given by the transmissivity, T_λ , of the layer. The transmissivity depends on the normal optical depth and the angle at which the beam deviates from straight down, the zenith angle θ . The transmissivity is defined by [Wallace & Hobbs, 2006]

$$T_\lambda = e^{-\tau_{norm} \sec \theta} \quad (2.22)$$

It is obvious that T_λ decreases with increasing θ . Since the Arctic is far North, the incoming solar radiation is at a high zenith angle, and less SW reaches the surface than at lower latitudes. Consequently the SW reaching the surface in the Arctic is low compared to lower latitudes. Low clouds have a net cooling effect globally, due to their high albedo. In section ?? it was shown that clouds not only reflect SW radiation, but also emit LW radiation. When there is little SW to reflect, the warming effect of the emission of LW radiation is enhanced.

Clouds in the Arctic are mostly optically thin and low lying [Curry *et al.*, 1996].

The clouds studied in this thesis are low (up to about 1600 m) stratus clouds, in the Arctic. Stratus clouds are low layered clouds that form when extensive areas of stable air is lifted. They are normally between 0.5 and 1 km thick, and can be several km wide [Aguado & Burt, 2010]. The largest amounts of low stratus clouds in the Arctic are over the ocean [Klein & Hartmann, 1993]. According to Klein & Hartmann [1993] stratus in the Arctic basin peaks during summer at nearly 62%, while during the winter season the stratus only accounts for 18% of the cloud cover. This leads them to conclude that the seasonal cycle of stratus in the Arctic is driven by the temperature cycle, thereby moisture content in the atmosphere, rather than the static stability.

As mentioned in Chapter 1 there is no solar radiation to reflect during winter and the polar night in the Arctic, whereas in the summer the zenith angle is so high that even though there is sunlight 24 hours a day the cooling effect in summer does not average out the heating effect the clouds have in winter. A high zenith angle, means that the radiation has to travel through more atmosphere, which gives a higher optical depth and stronger depletion of the radiation beam. Consequently, the low clouds' ability to absorb and emit terrestrial radiation dominates over their reflective effect on the solar radiation.

The stratus clouds in the Arctic are typically thin (check with Curry@). The air in the Arctic is very stable in winter (polar night), and clean since there are not many sources for pollution. In Autumn the sea ice extent reaches a minimum after the summer melt and leaves open water to influence low clouds and their properties. Some of the cloud radiative properties are presented in the next section.

The tools and methods used to study Arctic clouds in this thesis are described in the following chapter.

Chapter 3

Model and methods

To produce results for the thesis, a formulation of the Weather Research and Forecasting (WRF) Model called the Advanced Research WRF (ARW) has been used. The model is described in the first part of this chapter. Then follows a description of the model setup and the different physics schemes that were chosen for this study, before a summary of the different runs that were performed. Ending the chapter are two short sections on the input data and processing of the model output.

3.1 Description of the WRF-ARW Modeling System

The version of the WRF-ARW modeling system used is 3.6.1, which was released in April 2014. The model is primarily developed at the National Centre for Atmospheric Research (NCAR) in Boulder, Colorado. The ARW model is the first fully compressible conservative form nonhydrostatic model designed for both research and operational numerical weather prediction (NWP) applications [Skamarock & Klemp, 2008].

As can be seen from figure 3.1 the WRF-ARW Modeling System consists of four major programs [Wang *et al.*, 2015]:

- The WRF Preprocessing System (WPS)
- WRF-Data Assimilation (WRF-DA)
- ARW solver
- Post-processing & Visualization tools

WPS is used primarily for real data simulations [Wang *et al.*, 2015], like the study presented in this thesis. A real-data simulation means that it has been initialized by observations and reanalysis, not artificial data. WPS' functions include defining simulation domains, interpolating terrestrial data

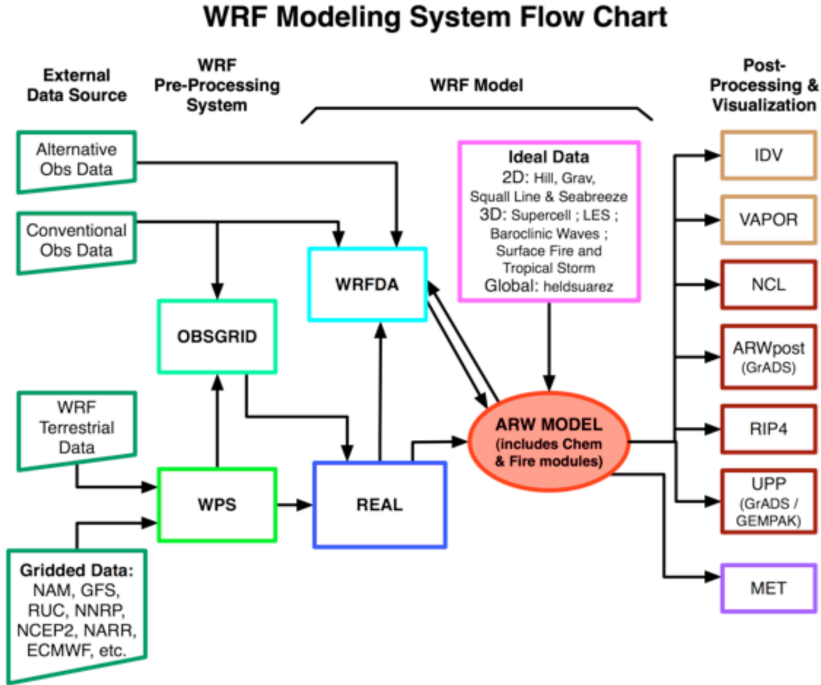


Figure 3.1: Flowchart for the WRF ARW Modeling System Version 3. From Wang *et al.* [2015].

and degridding and interpolating meteorological data from another model to this simulation domain [Wang *et al.*, 2015]. WRF-DA is optional and can be used to ingest observations into the interpolated analyses created by WPS [Wang *et al.*, 2015], but was not used in this study. The ARW solver is the key component of the modeling system, which is composed of several initialization programs for idealized, and real-data simulations, and the numerical integration program [Wang *et al.*, 2015].

3.1.1 The vertical coordinate

The continuous equations solved in the ARW model are the Euler equations cast in a flux form where the vertical coordinate, η , is defined by a normalized hydrostatic pressure,

$$\eta = (p_h - p_{ht})/\mu \quad (3.1)$$

where $\mu = (p_{hs} - p_{ht})$ [Skamarock & Klemp, 2008]. p_h is the hydrostatic component of the pressure and p_{hs} and p_{ht} are the values of the hydrostatic pressure in a dry atmosphere at the surface and top boundaries respectively [Skamarock & Klemp, 2008].

The vertical coordinate is the traditional σ coordinate used in many

hydrostatic atmospheric models, shown in figure 3.2.

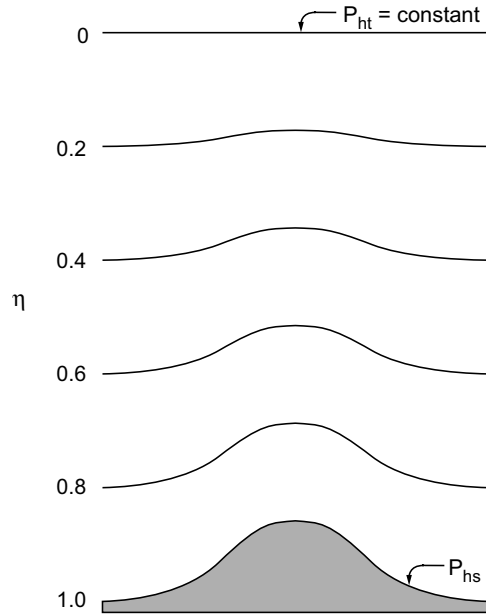


Figure 3.2: This figure is shown as presented in Skamarock & Klemp [2008], and is a schematic of the terrain following a σ coordinate. P_{hs} and P_{ht} are the hydrostatic pressure at the surface and top respectively.

3.1.2 Staggered grid

The WRF-model uses a staggered grid, which means that some variables lie in the middle of a grid box, and others on the sides of the box. The pressure for example is in the middle of the grid box, and the winds on each side of the box use the pressure in the middle of one box, and the middle of the box next to it as reference for calculating the winds at the grid box sides. A staggered grid saves computational time since a variable at point a needs only the values at $a+1/2$, and $a-1/2$, in stead of $a+1$ and $a-1$, which is more computationally costly.

The staggered grid therefore reduces the computation time of the WRF-ARW modeling system.

This is important to know, also for the variables in the vertical. If a cloud effective radius, r_e , for example lies between two levels, in the middle of a layer, or if they have values exactly on the levels.

Figure 3.3 shows the staggered C-grid used in the WRF-model. The C-grid is the most used staggered grid in nonhydrostatic NWP and research models [Skamarock & Klemp, 2008].

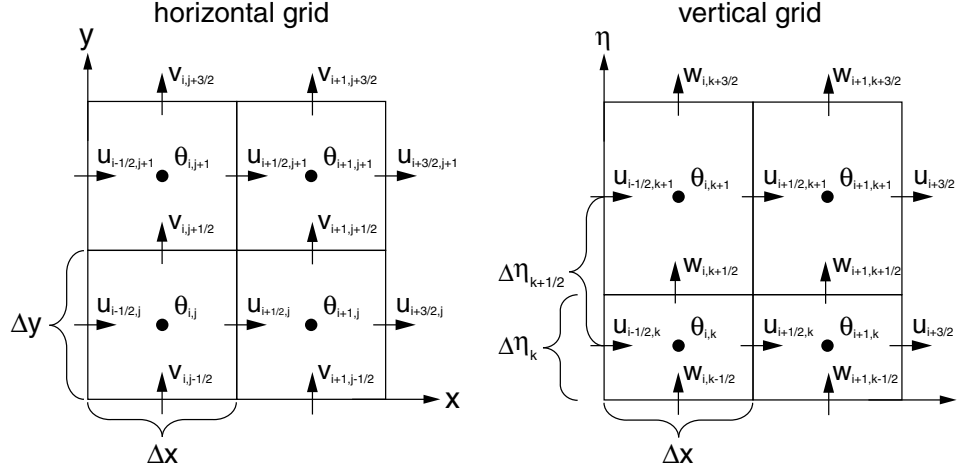


Figure 3.3: This figure is shown as presented in Skamarock & Klemp [2008], and shows the staggering for the C-grid. The horizontal staggering to the left, and the vertical staggering to the right.

The selection of physics schemes in WRF-ARW are numerous. The choice of schemes treating microphysics in clouds and aerosols, and the radiation are presented in the following section about the model setup.

3.2 Model setup

The model was ran with a $4 \text{ km} \times 4 \text{ km}$ horizontal grid point spacing, with 300×300 grid points, and 72 vertical layers, with the model top at 10 hPa. The area covers parts of the Beaufort Sea, by Canada and Alaska. This area was chosen because data from the area has been used for related studies [Intrieri *et al.*, 2002a, Kay & Gettelman, 2009, Palm *et al.*, 2010, Schweiger *et al.*, 2008, Shupe & Intrieri, 2004, Wu & Lee, 2012] as mentioned in Chapter 1. The area is not completely ice free any part of the year, and provides a good place to simulate cloud-sea ice interaction. The area is over several time zones but is approximately 7 hours behind UTC time. The times given in the WRF-ARW modeling system are UTC. The model was ran for a period of 5 days, 1st to 6th of September 2012. This is approximately when the record low ice extent in the Arctic was set (eg. National Snow and Ice Data Centre, U.S.A., Beitaler [2012]).

The vertical layers in the ARW model are often referred to as eta levels, because of the choice of η as the vertical coordinate. These levels have uneven vertical spacing. The fact that this η is the traditional σ -coordinate, means that the altitude of each level is dependent on pressure, therefore the level height varies in both time and space. As a consequence of pressure dependence, the levels in the lower troposphere are closer to each other than

the levels higher up in the troposphere. Therefore the low clouds in the area can be resolved. Approximate heights for the lowest 11 eta levels is shown in Table 3.1.

Table 3.1: Approximate height for each level in meters above the surface.

Eta level	Approximate height
1	10 m
2	50 m
3	130 m
4	230 m
5	370 m
6	530 m
7	650 m
8	950 m
9	1250 m
10	1400 m
11	1600 m

3.2.1 Choices of physics in the model

The physics options in WRF fall into several categories, each containing several choices. Table 3.2 shows some of the different categories and the choice of scheme, for this study, within each of those categories.

Table 3.2: Table of physics categories and choice of scheme for this thesis

Physics categories	Scheme selected within category
(1) microphysics	aerorol-aware [Reisner <i>et al.</i> , 1998, Thompson & Eidhammar, 2014, Thompson <i>et al.</i> , 2004, 2008]. Option 28.
(2) cumulus parameterization	Grell 3D @cite authors. Option 5.
(3) planetary boundary layer (PBL)	Yonsei University scheme @cite authors. Option 1.
(4) land-surface model	Noah Land Surface Model @cite authors. Option 2.
(5) radiation	RRTMG LW & SW [Iacono, 2003, Iacono <i>et al.</i> , 2000, 2008, Mlawer <i>et al.</i> , 1997]. Radiation options 4.

The ARW model offers a wide selection of schemes to treat different physics that one wants represented in the model. The schemes treat the physics slightly differently and some schemes are better for certain horizontal and vertical resolutions than others, so one needs to be careful when choosing

how the model is to treat the physics. For my thesis, the especially relevant scheme to mention is the cloud microphysics scheme that I chose, which is the aerosol-aware scheme described in Thompson & Eidhammer [2014]. When studying cloud and radiation response to removal of sea ice we might expect an increase in aerosols from the open ocean and increased sea traffic. The aerosols are therefore also relevant for the choice of schemes, and the aerosol-aware scheme includes the necessary processes for this study.

The aerosol-aware scheme

The microphysics includes explicitly resolved water vapor, cloud, and precipitation processes. The aerosol-aware scheme was chosen so that the study would have scavenging of aerosols included and have proper enough representation of aerosols to study aerosol-cloud interactions, without using the WRF model coupled with chemistry (WRF-Chem). According to the ARW User's Guide by Wang *et al.* [2015], the aerosol-aware scheme considers water- and ice-friendly aerosols, and a climatological dataset may be used to specify initial and boundary conditions for the aerosol variables. I have used this climatological dataset, which is explained in Section 3.4 Input data. The scheme uses a monthly mean for aerosol number concentrations derived from multi-year (2001-2007) global model simulations in which particles and their precursors are emitted by natural and anthropogenic sources and are explicitly modeled with multiple size bins for multiple species of aerosols by the Goddard Chemistry Aerosol Radiation and Transport (GOCART) model [Thompson & Eidhammer, 2014]. The aerosol-aware scheme [Thompson & Eidhammer, 2014] is built on the schematic shown in figure 3.4, from Reisner *et al.* [1998]. It is a double moment scheme, which means it computes both mass mixing ratios, Q , and number concentrations, N , for the same water species (hydrometeors).

Figure 3.4 show the processes in the microphysics scheme developed by Reisner *et al.* [1998], which the first bulk microphysics scheme by Thompson [Thompson *et al.* , 2004] was based on. The aerosol-aware scheme [Thompson & Eidhammer, 2014] is an extension of the updated Thompson bulk microphysics scheme described in Thompson *et al.* [2008]. The figure shows a schematic of five hydrometeors, cloud water (c), rain (r), ice (i), snow (s) and graupel (g), and if just the mass mixing ratio is calculated or if both the mass mixing ratio and the number concentration is calculated. For each of the hydrometeors, prognostic equations are used with all the sources and sink terms included.

The RRTMG radiation schemes

According to Thompson & Eidammer [2014] the Rapid Radiative Transfer Model (RRTM) for General Circulation Models (GCMs) (RRTMG) schemes

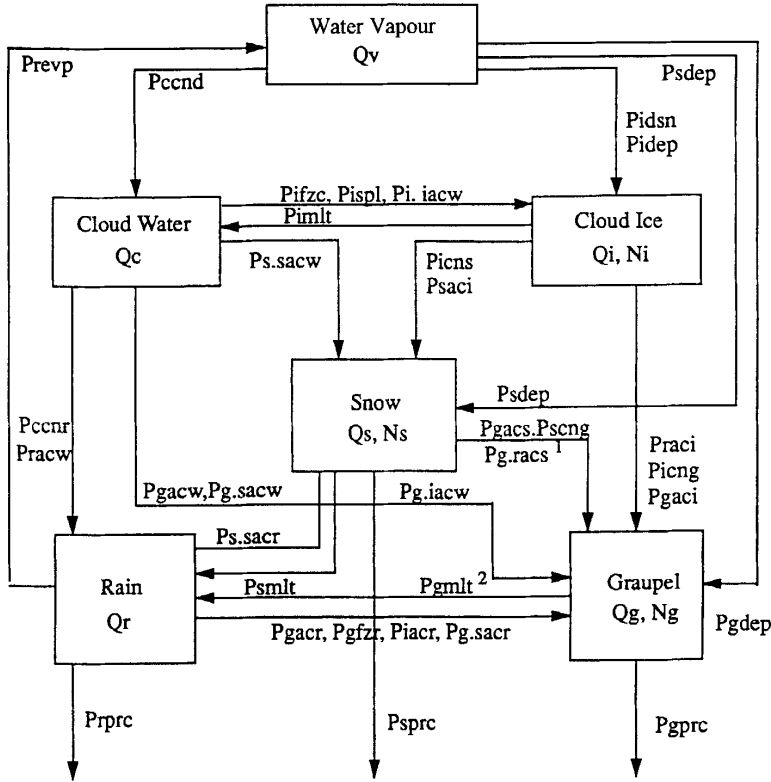


Figure 3.4: Cloud microphysical parameterization scheme typically used in NWP models as shown in Reisner *et al.* [1998]. A full list of the acronyms used in the schematic can be found in Reisner *et al.* [1998].

for SW and LW [Iacono, 2003, Iacono *et al.*, 2000, 2008, Mlawer *et al.*, 1997] are the only radiation schemes which include the effects of the effective radii calculated in aerosol-aware. These were therefore used in combination with the aerosol-aware cloud microphysics scheme. The RRTMG schemes are accurate schemes using look-up tables for efficiency, and accounts for multiple bands and microphysics species, and includes the Monte Carlo Independent Column Approximation (MCICA) method of random cloud overlap [Wang *et al.*, 2015].

3.3 Model runs

The results presented in the next chapter are based on six different runs. The control run is the run where the aerosol climatological dataset has been used unchanged, and where the sea ice is kept as it was in the downloaded input data, see Section 3.4. The control run is used as a base to compare the other runs to, those with no ice and/or increased aerosol number concentrations.

There are three runs where the sea ice was removed, NoIce, Aero10NoIce and Aero100NoIce. The point of this is to compare the run with no ice to the control run, and see if there are any changes in the cloud properties, and SW and LW fluxes. For two of those runs the aerosol number concentration was also increased, these can be compared with the control run, and the other runs that have ice, but the same aerosol number concentrations.

The number of water- and ice-friendly aerosols were multiplied by 10 and 100 both with and without sea ice for 4 runs in total: Aero10 and Aero100 with ice, and as mentioned above, Aero10NoIce and Aero100NoIce without ice. The goal is to find changes in cloud properties, and radiation fluxes compared to those in the control run.

Table 3.3 shows an overview of the different runs that have been executed, whose output have been used for production of figures presented in the next chapter.

Table 3.3: Table showing the names of the runs and if they have sea ice or not, and if the aerosol concentration has been increased by a factor of 10 or 100 through input files. All the runs have the same horizontal resolution of $4 \text{ km} \times 4 \text{ km}$, dimensions 300×300 , 72 vertical layers and time step 24 s.

Name	Sea ice	Aerosol concentration
control	initial	climatology
NoIce	removed	climatology
Aero10	initial	climatology $\times 10$
Aero10NoIce	removed	climatology $\times 10$
Aero100	initial	climatology $\times 100$
Aero100NoIce	removed	climatology $\times 100$

3.3.1 Manipulation of input files

The input files for the ARW solver, created by WPS and REAL (see figure 3.1) were manipulated by use of the NetCDF Operator (NCO) tool ncap2. In these files the sea ice was removed for the runs without sea ice (NoIce, Aero10NoIce, Aero100NoIce) and the aerosol number concentration from the climatological dataset was multiplied by 10 and 100 for the runs with increased aerosol concentrations by a factor of 10 and 100 respectively.

3.4 Input data

The model runs were initialized with data downloaded from the European Centre for Medium-Range Weather Forecasts (ECMWF). The downloaded

data is from the ERA-Interim dataset, which is a global atmospheric reanalysis from 1979 to present and continues to be updated in real time. Through WPS the data from ERA-Interim was interpolated over the area, with a 2 degree minute spacing between the points, to be used to initialize the model. The data used is in 6-hourly atmospheric fields on pressure levels, for the first five days of September 2012, which was the period the model was run for. This is done to make sure the initial meteorological conditions are the same in every run, so that the effects of changing a variable in the input files for the modeling system are only due to that change.

To use the climatological aerosol dataset, the file containing monthly means had to be called through WPS. The aerosol input data includes mass mixing ratios of sulfates, sea salts, organic carbon, dust, and black carbon from a 7-yr simulation with 0.5° longitude by 1.25° latitude spacing [Thompson & Eidhammer, 2014].

3.5 Processing of the results

Figures presented in my thesis, I made (unless other is stated) by use of NCL (National Centre for Atmospheric Research (NCAR) Command Language) and/or MatLab. For the NCL scripts I found a lot of help and inspiration from the example scripts for WRF-users available at ([URL for examples](#)).

Chapter 4

Results and discussion

In this chapter I will present the findings made in this thesis.

4.1 Reference figures from the control run

First we want to have something to compare with and to look back to when studying the differences from the control run to the runs with changed sea ice and/or aerosol concentration. I shall include figures for diurnally averaged fields of LWP, r_e of cloud droplet, cloud droplet number concentration (CDNC), both LW and SW up at the TOA and down at the surface. Also the IWP, cloud ice number concentration (CINC), and r_e of snow and ice may be of interest. In addition, the state of the weather situation should be considered when interpreting the results. Therefore maps with wind barbs for the wind at 10 m height and temperature at 2 m are included in this section. (*De ligger i slutten av kapittelet foreløpig, slik at de ikke er i veien for leseren utover i teksten.*)

4.2 Removed sea ice

4.2.1 Day 2

Lets start with average difference in LWP for NoIce - Control, day 2 (see figure 4.1). (*day 1 has been left out of this discussion to avoid the spin-up time. I want to look more closely into day 1 as well, which is when the atmosphere is still almost the same as it was for the control run, will be included in next draft.*) There is a slight difference in LWP for the whole field (2.04gm^{-2} , see figure 4.1), but the area of interest in this case is where the sea ice is no longer present. There the increase in LWP is significantly higher, $>25\text{gm}^{-2}$ for the most northern part (which is in the bottom right corner). This implies that there is a new cloud forming in that area, that could not form when there was sea ice. The removal of the sea ice has allowed

for increased evaporation and an increase in latent heat (LH) flux which can be seen from figure 4.2, where the area that sea ice was removed from is obvious. The northernmost part of the study area also has an increase in the cloud droplet number concentration (CDNC), figure 4.1, with about the same shape and size as the LWP, which fits well with equation 4.1, which we know from the theory presented in chapter 2.

$$LWC = \frac{4}{3} \pi \rho r_e^3 N \quad (4.1)$$

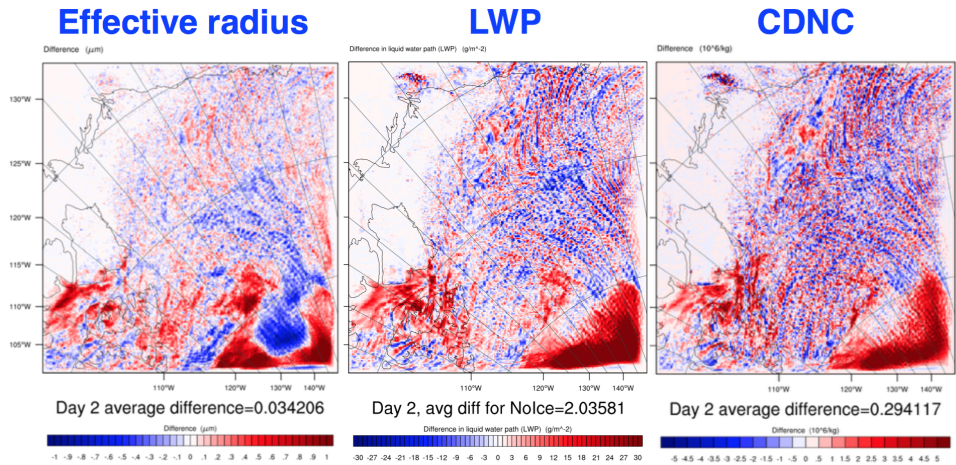


Figure 4.1: The averaged difference in r_e of cloud droplets, LWP and CDNC (from left to right) for the run with no ice, over the lowermost 11 layers for day 2. (preliminary figure)

The amount of liquid water is proportional to the number concentration, and the LWP is the integral over the LWC, where we recall that N is the CDNC. The average increase in the CDNC would be approximately 5 droplets per cubic centimeter. The figure shows the numbers with units $10^6/kg$, which can be approximated to the more common units for CDNC, per cubic centimeter (cm^{-3}). If we assume that we are close enough to the surface to assume a pressure $p = 1000hPa$, and thereby the density to be $\rho_a = 1kg/m^3 = 1kg/10^6cm^3$, then we could write $CDNC : 10^6/kg = cm^{-3}$. Since this is the average over 11 layers, to a height of about 1600 m, the cloud could be in just a few of those layers, and have a CDNC of approximately 25 cm^{-3} if it stretches over two layers for example. The increase in effective radius in the same area also indicates the formation of a new cloud, figure 4.1, that could not form in the control run (see figure 4.20), whereas now that it has formed, the droplets actually have a radius. The small "blob" at $140^\circ W$ and about $81^\circ N$ has decreased r_e , most likely because the cloud already was saturated in that area, which can be seen from the

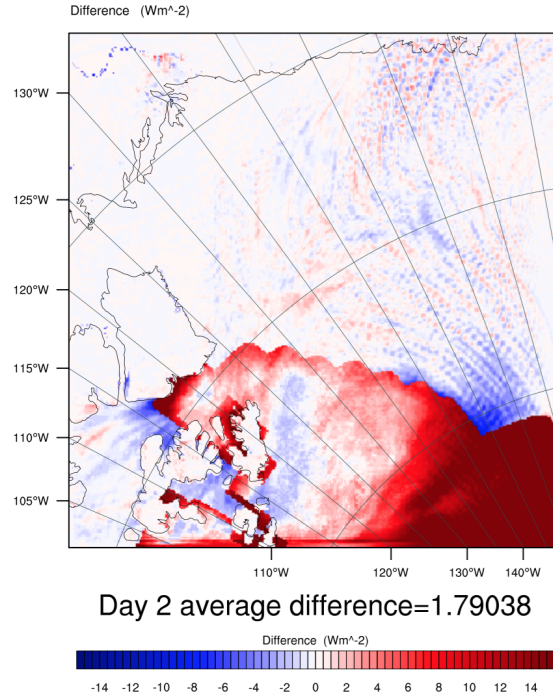


Figure 4.2: The average difference in LH flux up from the surface at day 2 .

LWP from the control run, in figure 4.18. The possible increase in aerosols from the ocean that would then lead to an increase in CCNs would make the water in that cloud spread over more CCNs, and by that leave the droplets with a smaller r_e .

The kind of U-shape that we can see in the figure for difference in r_e , figure 4.1, is also clear in the difference in downward radiation at the ground surface, for both SW and LW. The SW radiation flux at ground surface has been reduced, which is due to the increase in LWP. This can be explained by equations 2.6 and 2.19, where it is clear from equation 2.19 that the cloud optical depth, τ_{sw} , increases with LWP, and from equation 2.6 it is clear that an increase in τ_{sw} would also increase the cloud albedo.

The downward LW radiation flux at the surface has been increased due to the increase in LWP, which means that there is more water in the clouds and they emit more LW to the ground. It was shown in Chapter 2 that an increase in LWP increases the cloud optical depth also in the LW, see equation ??, which in turn increases the emissivity of the cloud, shown in equation 2.2. The LW at the top of the atmosphere (TOA) does not experience such an increase, in fact it experiences a slight decrease. That it doesn't experience the same increase is explained by the Stefan-Boltzmann's law presented in chapter 2, where the flux density emitted by a body, in this case a cloud, is dependent on the temperature. *We see from the*

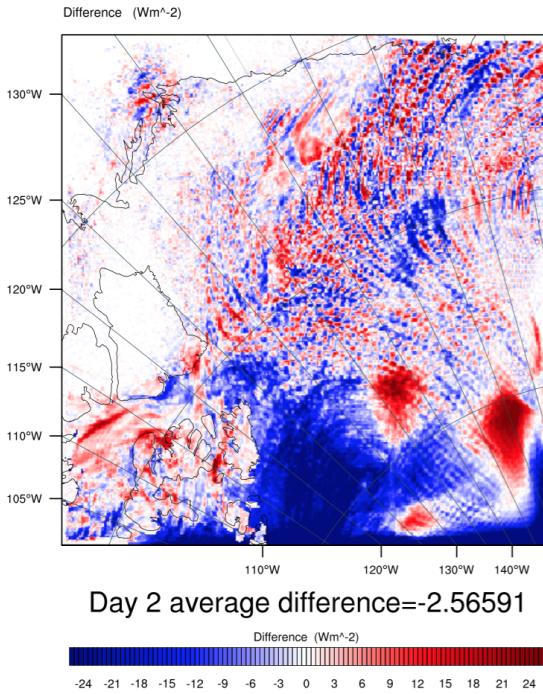


Figure 4.3: The average difference in SW flux up at TOA at day 2 .

vertical cross section showing temperature contours (@refer and make), that the temperature is higher at the surface than in the clouds, therefore the clouds have a lower emittance of LW. (this figure will come in the next draft, but is currently not averaged)

Of course, the removal of sea ice would reduce the reflected SW radiation flux at the TOA, see figure 4.3. The albedo of sea ice varies between 0.5 and 0.9 depending on snow cover and the age of the ice and is typically 0.5-0.7 for bare ice, whereas a typical ocean albedo is 0.06. Thus the change in SW at TOA is mainly negative over the area of ocean where there was sea ice in the control run. The two blobs of increased SW at TOA, see figure 4.3, can be recognized as the tips of the pillars in the U-shape I referred to for r_e earlier (in figure 4.1) which also represent an increase in LWP and reduction in SW at surface and increase of LW at surface. This is therefore most likely due to the enhanced albedo caused by new clouds at those locations, since these figures don't show in-cloud changes, simply the difference between two fields.

The heat fluxes are almost unchanged for most of the study area by the removal of sea ice, except for the area where the sea ice has been removed (see figures 4.2 and 4.4). Especially for the northernmost part of the study area and "sea ice removed area" the fluxes are a lot higher than in the control run. This is not surprising, since one would expect the ocean surface

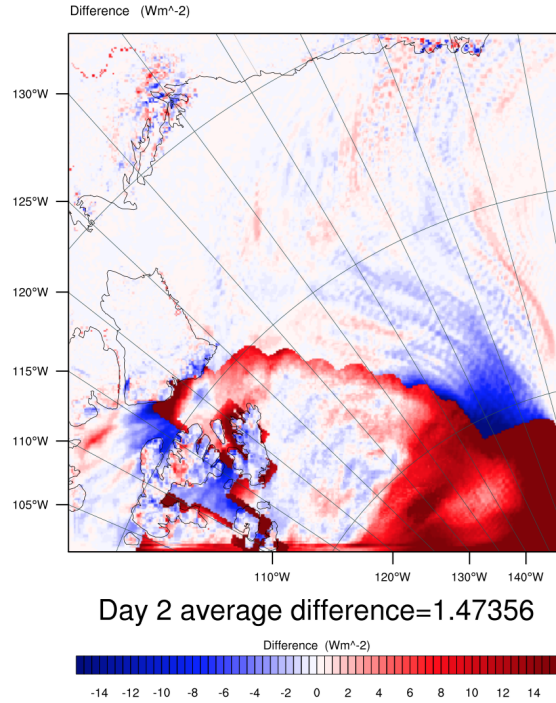


Figure 4.4: The average difference in SH flux up from the surface at day 2 .

to hold a higher temperature than the sea ice. Also a lot more heat would be released due to evaporation than in the case when sea ice is present.

4.2.2 Day 5

I still can't explain what is going on in figure 4.5. I have tried to look into differences in rain, and snow, and graupel and ice content, but I can't seem to figure it out...

4.3 Increased aerosol concentration

4.3.1 Day2

The increase in available CCNs leads to obvious increases in CDNC and LWP, and the expected reduction in r_e , see figure 4.6.

As for the NoIce run, the increase in LWP, in this case a lot higher, leads to an increase in clouds and their reflectance (albedo), therefore the SW at TOA is higher, here the signal is not disrupted by any changes made to the sea ice, so the increase is obvious, and is shown in figure 4.7. Thus the SW at the surface is significantly lower than in the control run. This represents a cooling of (@calculate the flux changes into temperature changes?). The

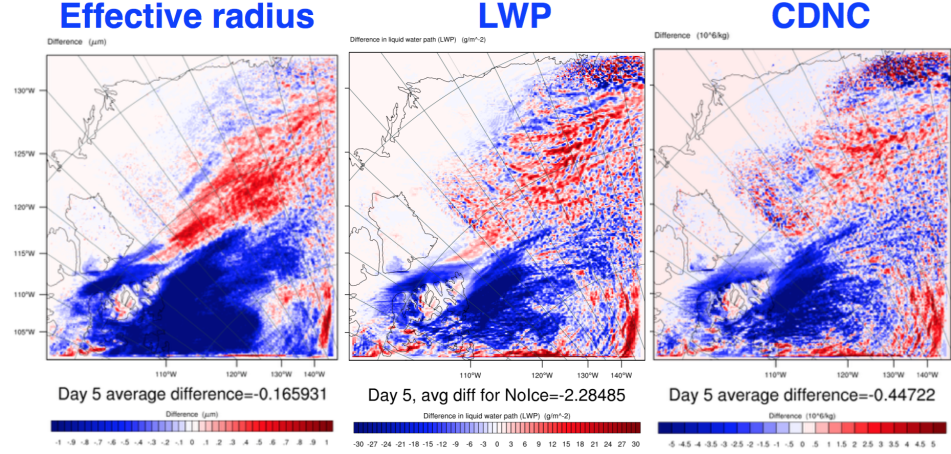


Figure 4.5: The average differences in r_e , LWP and CDNC from left to right, for day 5. (preliminary figure)

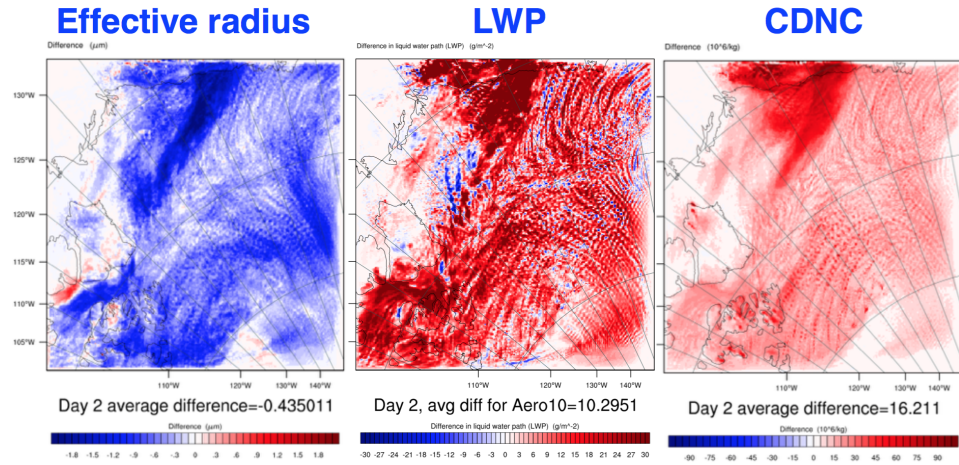


Figure 4.6: The average differences in r_e , LWP and CDNC from left to right, for day 2. (preliminary figure)

average LW radiation flux at the surface is higher due to the increase in LWP and thereby increased emittance by the clouds. The effect on the heat fluxes by increasing the aerosol number concentration is not clear, and probably insignificant (not shown).

4.3.2 Day 5

The LW cloud emissivity is sensitive to an increase in water amount as long as the LWP is less than $\approx 40\text{-}45 \text{ g/m}^2$. It is clear in day 5 from the control run that the LWP was around $60\text{-}100 \text{ g/m}^2$ in the middle lower area

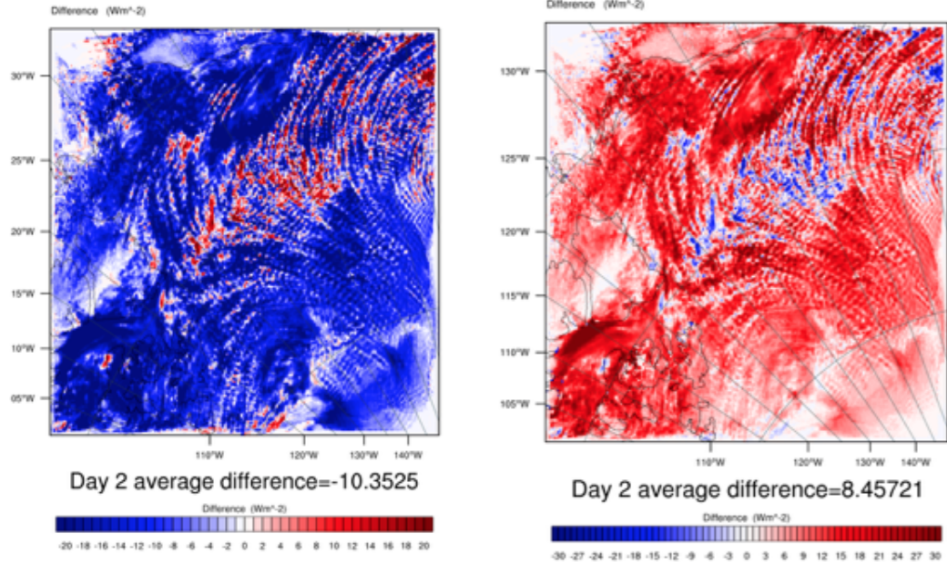


Figure 4.7: The average difference in SW down at the surface, and up at TOA, from left to right, for day 2. (preliminary figure)

of figure 4.19. This is also seen in that there is no significant change in LW downward at the surface or upward at the TOA, see figure 4.8. The area with

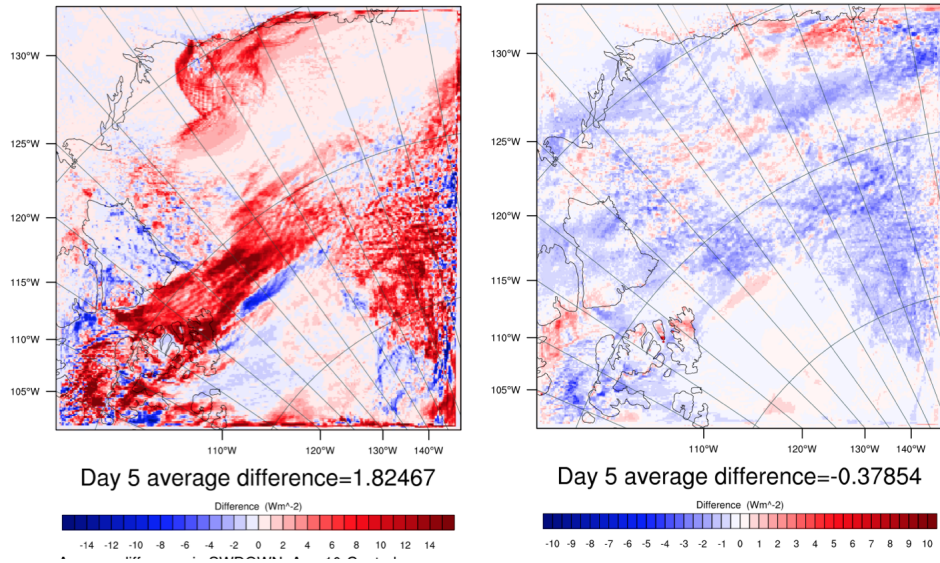


Figure 4.8: The average difference in LW downward at the surface and upward at TOA on day 5, from left to right. (preliminary figure)

lack of change in LW up or down is approximately the same area as where

there is a negative change in LH and SH upward from the surface over the sea ice, see figure 4.10. Since there has been no change in LW there is no loss of warming from a decrease in LW reaching the surface, but the change can possibly be explained by looking at the SW radiation. The downward SW at the surface has been significantly decreased as a consequence of the increase in aerosol number concentration, see figure 4.9. The SW radiation has been reflected by the smaller and more numerous droplets. This is known as the Twomey effect, and was described in Chapter 2.

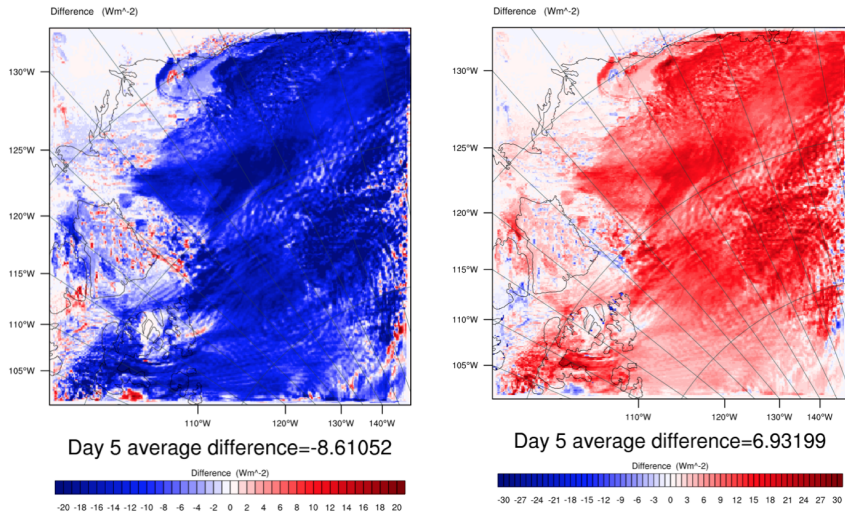


Figure 4.9: The average difference in SW downward at the surface, and upward on TOA at day 5, from left to right. (preliminary figure)

The albedo of sea ice is typically 0.5-0.7 which means that a fraction of the incident SW radiation is absorbed. Since the amount of incident SW radiation at the surface has been reduced by the cloud cover, the absorbed radiation is less than for a higher incident amount. The ice therefore has a lower temperature to give off SH with.

The skin temperature, figure 4.11, for the domain shows a small decrease in the same area as where there is less sensible and latent heat release.

Also the dynamics over ice and the ocean are different, so this could have an effect. The cold air over the ice may be intensified, while the sea surface temperature (SST) is the same for all the runs and there is no coupling with the ocean. There will therefore be no changes in the SSTs that could have an effect on the dynamics over the ocean. So the response may be smaller there...?

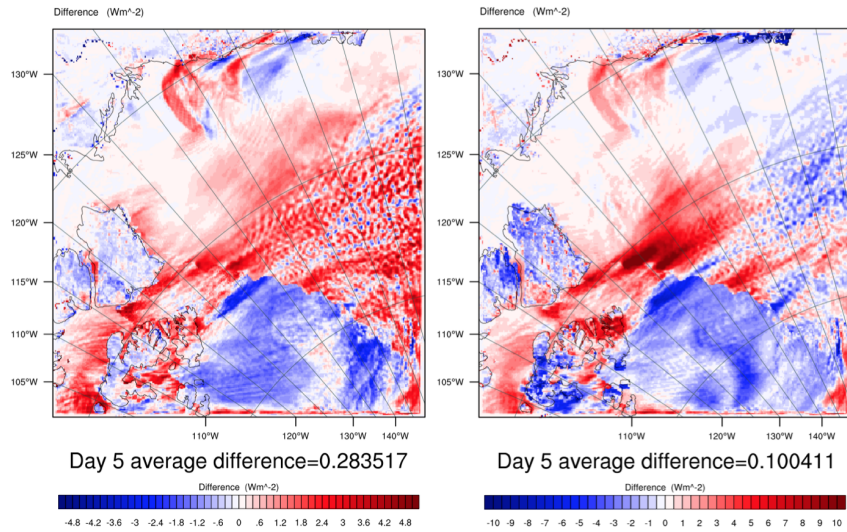


Figure 4.10: The average difference in LH and SH upward at the surface on day 5, from left to right. (preliminary figure)

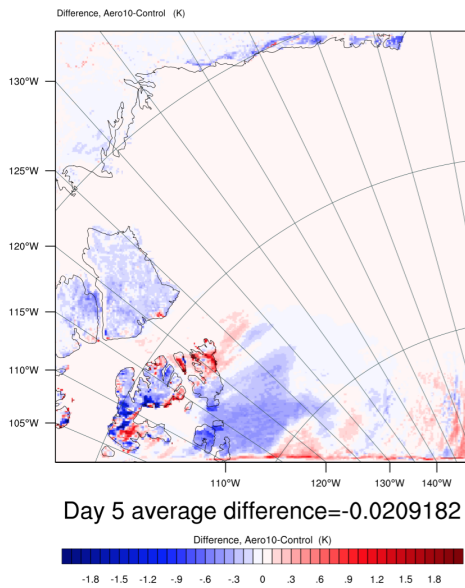


Figure 4.11: The average difference in skin temperature (the temperature of the surface), for day 5.

4.4 The control run figures

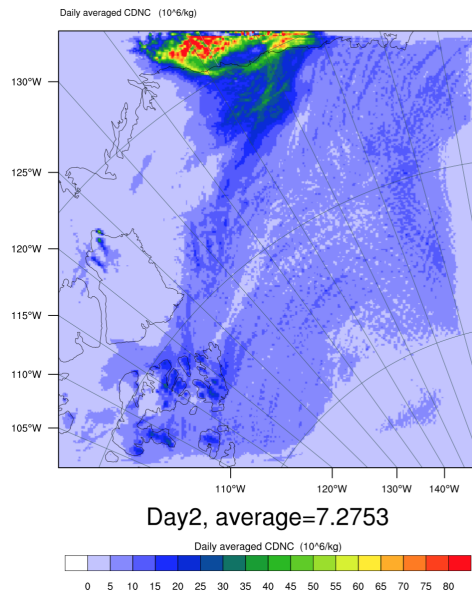


Figure 4.12: Cloud droplet number concentration, plotted over the area, averaged over the lower 11 layers on the 2nd day.

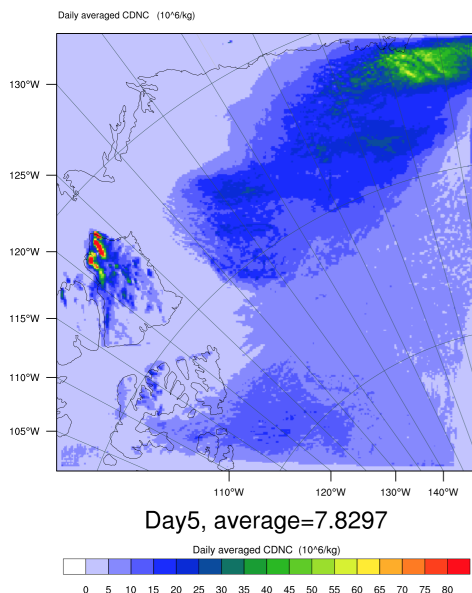


Figure 4.13: Cloud droplet number concentration, plotted over the area, averaged over the lower 11 layers on the 5th day.

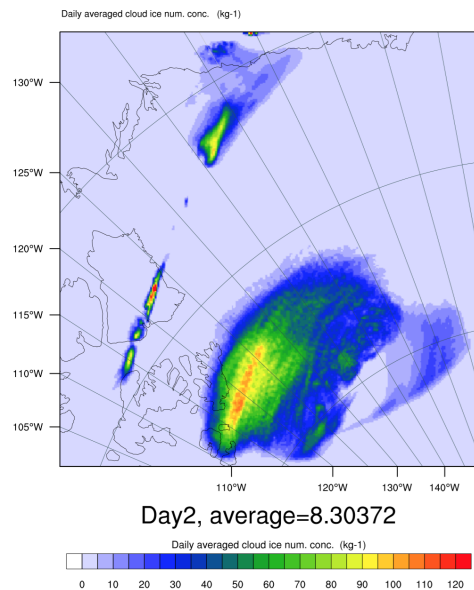


Figure 4.14: Cloud ice number concentration, plotted over the area, averaged over the lower 11 layers on the 2nd day.

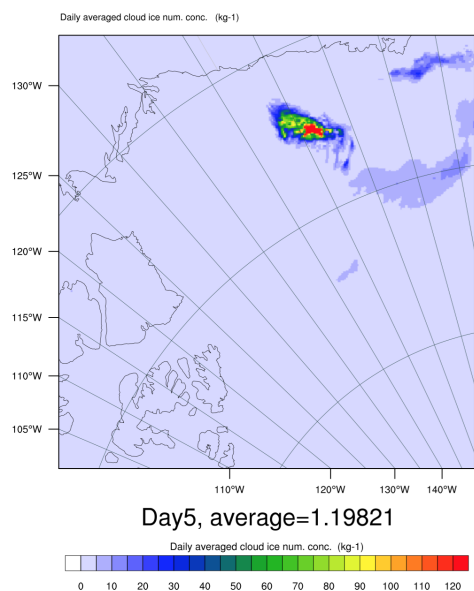


Figure 4.15: Cloud ice number concentration, plotted over the area, averaged over the lower 11 layers on the 5th day.

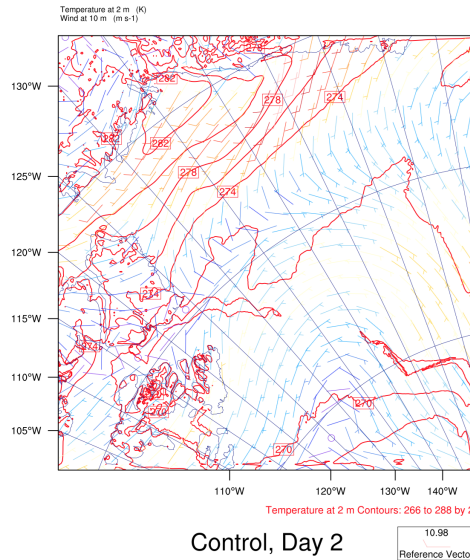


Figure 4.16: Map showing the mean wind at 10 m as wind barbs and mean temperature at 2 m as contours, for day 2 of the control run.

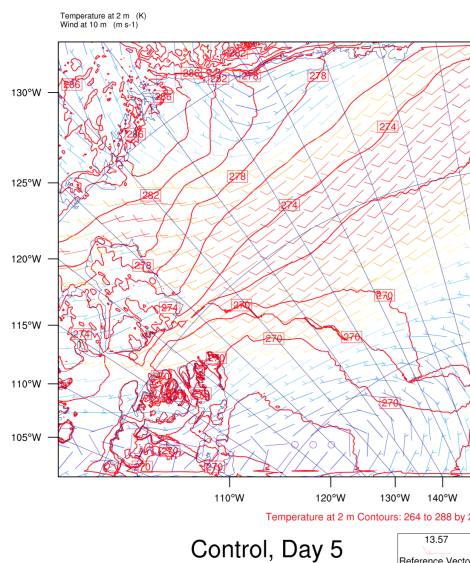


Figure 4.17: Map showing the mean wind at 10 m as wind barbs and mean temperature at 2 m as contours, for day 5 of the control run.

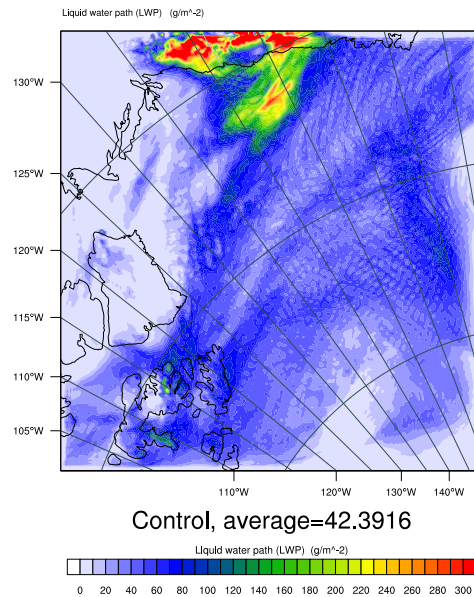


Figure 4.18: The liquid water path (LWP) average field for day 2 of the control run, with the average value for that field.

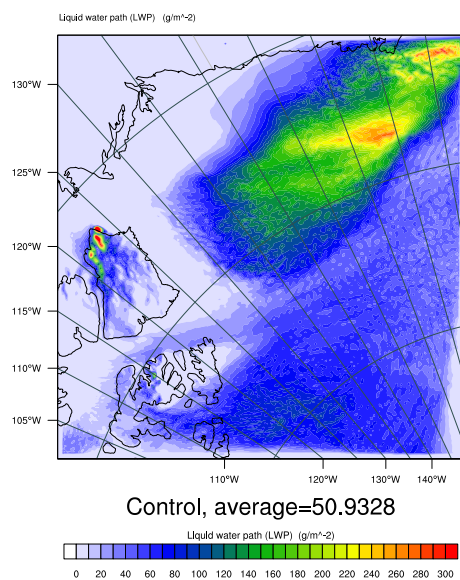


Figure 4.19: The liquid water path (LWP) average field for day 5 of the control run, with the average value for that field.

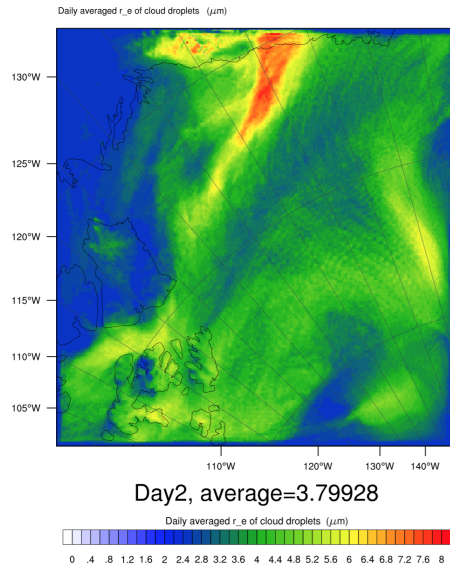


Figure 4.20: The effective radius of cloud droplets average field for day 2 over the lowermost 11 layers.

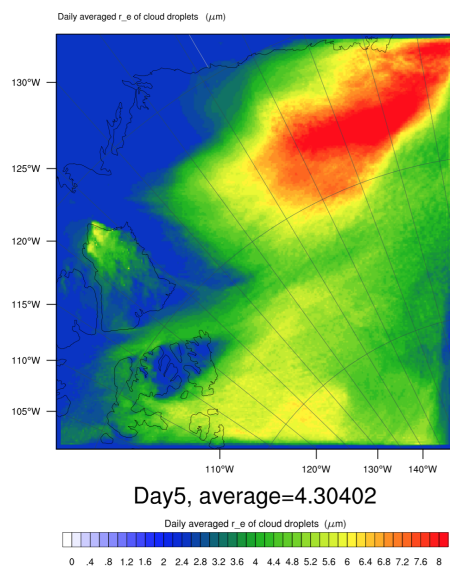


Figure 4.21: The effective radius of cloud droplets average field for day 5 over the lowermost 11 layers.

Chapter 5

Summary and Conclusions

In this thesis I have found things presented in the previous chapter, but it is still a bit too messy and incomplete to conclude anything.

Stuff to do:

- Kort oppsummering av hva som er gjort og hvorfor
- Kort oppsummering av resultater
- Kort tolkning av resultatene
- Sluttord (f.eks. videre forskning eller annet perspektiv)

Bibliography

- Aguado, Edward, & Burt, James E. 2010. *Understanding Weather and Climate*. 5th edn. Pearson Prentice Hall.
- Albrecht, Bruce A. 1989. Aerosols, Cloud Microphysics, and Fractional Cloudiness. *Science*, **245**(4923), 1227–1230.
- Beitler, Jane. 2012. Arctic sea ice extent settles at record seasonal minimum. *National Snow and Ice Data Centre U.S.A.*
- Boucher, O., Randall, David, Artaxo, P., Bretherton, C., Feingold, G., Forster, P., Kerminen, V.M., Kondo, Y., Liao, H., Lohmann, U., Rasch, P., Satheesh, S. K., Sherwood, S., Stevens, B., & Zhang, X. Y. 2013. Clouds and Aerosols. *Pages 571–657 of:* Stocker, T. F., Qin, D., Plattner, G.-K., Tignor, M., Allen, S.K., Boschung, J., Nauels, A., Xia, Y., Bex, V., & Midgley, P. M. (eds), *Climate Change 2013: The physical Science Basis. Contribution of Working Group I to the Fifth Assessment Report of the Intergovernmental Panel on Climate Change*. Cambridge University Press, Cambridge, United Kingdom and New York, NY, USA.
- Curry, J. a., Hobbs, P. V., King, M. D., Randall, D. a., Minnis, P., Isaac, G. a., Pinto, J. O., Uttal, T., Bucholtz, A., Cripe, D. G., Gerber, H., Fairall, C. W., Garrett, T. J., Hudson, J., Intrieri, J. M., Jakob, C., Jensen, T., Lawson, P., Marcotte, D., Nguyen, L., Pilewskie, P., Rangno, A., Rogers, D. C., Strawbridge, K. B., Valero, F. P J, Williams, a. G., & Wylie, D. 2000. FIRE arctic clouds experiment. *Bulletin of the American Meteorological Society*, **81**(1), 5–29.
- Curry, Judith A., Schramm, Julie L., Rossow, William B., & Randall, David. 1996. Overview of Arctic Cloud and Radiation Characteristics. *Journal of Climate*, **9**(8), 1731–1764.
- Eastman, Ryan, & Warren, Stephen G. 2010a. Arctic cloud changes from surface and satellite observations. *Journal of Climate*, **23**(15), 4233–4242.
- Eastman, Ryan, & Warren, Stephen G. 2010b. Interannual variations of arctic cloud types in relation to sea ice. *Journal of Climate*, **23**(15), 4216–4232.

- Graversen, Rune G, Mauritsen, Thorsten, Tjernström, Michael, Källén, Erland, & Svensson, Gunilla. 2008. Vertical structure of recent Arctic warming. *Nature*, **451**(7174), 53–56.
- Hansen, J. E., & Travis, L. D. 1974. Light scattering in planetary atmospheres. *Space Science Reviews*, **16**(1957), 527–610.
- Iacono, Michael J. 2003. Evaluation of upper tropospheric water vapor in the NCAR Community Climate Model (CCM3) using modeled and observed HIRS radiances. *Journal of Geophysical Research*, **108**(D2).
- Iacono, Michael J., Mlawer, Eli J., Clough, Shepard a., & Morcrette, Jean-Jacques. 2000. Impact of an improved longwave radiation model, RRTM, on the energy budget and thermodynamic properties of the NCAR community climate model, CCM3. *Journal of Geophysical Research*, **105**(D11), 14873.
- Iacono, Michael J., Delamere, Jennifer S., Mlawer, Eli J., Shephard, Mark W., Clough, Shepard a., & Collins, William D. 2008. Radiative forcing by long-lived greenhouse gases: Calculations with the AER radiative transfer models. *Journal of Geophysical Research: Atmospheres*, **113**(13), 2–9.
- Intrieri, J M, Shupe, M D, Uttal, T, & Mccarty, B J. 2002a. An annual cycle of Arctic cloud characteristics observed by radar and lidar at SHEBA. *Journal of Geophysical Research*, **107**(C10).
- Intrieri, J. M., Fairall, C. W., Shupe, M. D., Persson, P. Ola G, Andreas, E. L., Guest, P. S., & Moritz, R. E. 2002b. An annual cycle of Arctic surface cloud forcing at SHEBA. *Journal of Geophysical Research*, **107**(C10), 1–14.
- Kay, Jennifer E., & Gettelman, Andrew. 2009. Cloud influence on and response to seasonal Arctic sea ice loss. *Journal of Geophysical Research D: Atmospheres*, **114**(18).
- Klein, S. A., & Hartmann, D. L. 1993. The seasonal cycle of low stratiform clouds. *Journal of Climate*, **6**, 1587–1606.
- Liou, K. N. 2002. *An Introduction to Atmospheric Radiation*. 2nd edn. Academic Press.
- Lohmann, U., & Feichter, J. 2005. Global indirect aerosol effects: a review. *Atmospheric Chemistry and Physics Discussions*, **4**(6), 7561–7614.
- McDonald, James E. 1958. *The Physics of Cloud Modification*.

- Mlawer, Eli J., Taubman, Steven J., Brown, Patrick D., Iacono, Michael J., & Clough, Shepard a. 1997. Radiative transfer for inhomogeneous atmospheres: RRTM, a validated correlated-k model for the longwave. *Journal of Geophysical Research*, **102**(D14), 16663.
- Palm, Stephen P., Strey, Sara T., Spinhirne, James, & Markus, Thorsten. 2010. Influence of Arctic sea ice extent on polar cloud fraction and vertical structure and implications for regional climate. *Journal of Geophysical Research*, **115**(D21), D21209.
- Reisner, J., Rasmussen, R M., & Bruintjes, R T. 1998. Explicit forecasting of supercooled liquid water in winter storms using the MM5 mesoscale model. *Quarterly Journal of the Royal Meteorological Society*, **124**(548), 1071–1107.
- Rogers, R. R., & Yau, M. K. 1989. *A Short Course in Cloud Physics*. 3rd edn. Butterworth-Heinemann.
- Schweiger, Axel J., Lindsay, Ron W., Vavrus, Steve, & Francis, Jennifer A. 2008. Relationships between Arctic Sea Ice and Clouds during Autumn. *Journal of Climate*, **21**(18), 4799–4810.
- Shupe, Matthew D., & Intrieri, Janet M. 2004. Cloud radiative forcing of the Arctic surface: The influence of cloud properties, surface albedo, and solar zenith angle. *Journal of Climate*, **17**(3), 616–628.
- Skamarock, William C., & Klemp, Joseph B. 2008. A time-split nonhydrostatic atmospheric model for weather research and forecasting applications. *Journal of Computational Physics*, **227**(7), 3465–3485.
- Stevens, Bjorn, & Feingold, Graham. 2009. Untangling aerosol effects on clouds and precipitation in a buffered system. *Nature*, **461**(7264), 607–613.
- Stevens, Björn, & Seifert, Axel. 2008. Understanding macrophysical outcomes of microphysical choices in simulations of shallow cumulus convection. *Journal of the Meteorological Society of Japan*, **86A**(August 2006), 143–162.
- Thompson, Gregory, & Eidhammer, Trude. 2014. A study of aerosol impacts on clouds and precipitation development in a large winter cyclone. *Journal of the Atmospheric Sciences*, 140507124141006.
- Thompson, Gregory, Rasmussen, Roy M., & Manning, Kevin. 2004. Explicit Forecasts of Winter Precipitation Using an Improved Bulk Microphysics Scheme. Part I: Description and Sensitivity Analysis. *Monthly Weather Review*, **132**, 519–542.

- Thompson, Gregory, Field, Paul R., Rasmussen, Roy M., & Hall, William D. 2008. Explicit Forecasts of Winter Precipitation Using an Improved Bulk Microphysics Scheme. Part II: Implementation of a New Snow Parameterization. *Monthly Weather Review*, **136**, 5095–5115.
- Twomey, S. 1974. Pollution and the Planetary Albedo. *Atmospheric Environment*, **8**, 1251–1256.
- Twomey, S. 1977. The Influence of Pollution on the Shortwave Albedo of Clouds. *Journal of the Atmospheric Sciences*, **34**, 1149–1152.
- Uttal, Taneil, Curry, Judith a., Mcphee, Miles G., Moritz, Donald K. Perovich Richard E., Maslanik, James a., Guest, Peter S., Stern, Harry L., Moore, James a., Turenne, Rene, Heiberg, Andreas, Serreze, Mark. C., Wylie, Donald P., Persson, Ola G., Paulson, Clayton a., Halle, Christopher, Morison, James H., Wheeler, Patricia a., Makshtas, Alexander, Welch, Harold, Shupe, Matthew D., Intrieri, Janet M., Stamnes, Knut, Lindsey, Ronald W., Pinkel, Robert, Pegau, W. Scott, Stanton, Timothy P., & Grenfeld, Thomas C. 2002. Surface heat budget of the Arctic Ocean. *Bulletin of the American Meteorological Society*, **83**, 255–276.
- Vavrus, Steve, Holland, Marika M., & Bailey, David A. 2010. Changes in Arctic clouds during intervals of rapid sea ice loss. *Climate Dynamics*, **36**, 1475–1489.
- Verlinde, J., Harrington, J. Y., McFarquhar, G. M., Yannuzzi, V. T., Avramov, a., Greenberg, S., Johnson, N., Zhang, G., Poellot, M. R., Mather, J. H., Turner, D. D., Eloranta, E. W., Zak, B. D., Prenni, a. J., Daniel, J. S., Kok, G. L., Tobin, D. C., Holz, R., Sassen, K., Spangenberg, D., Minnis, P., Tooman, T. P., Ivey, M. D., Richardson, S. J., Bahrmann, C. P., Shupe, M., DeMott, P. J., Heymsfield, a. J., & Schofield, R. 2007. The mixed-phase arctic cloud experiment. *Bulletin of the American Meteorological Society*, **88**(2), 205–221.
- Wallace, John M., & Hobbs, Peter V. 2006. *Atmospheric Science, An Introductory Survey*. 2nd edn. Academic Press.
- Wang, Wei, Bruyère, Cindy, Duda, Michael, Dudhia, Jimy, Gill, Dave, Kavulich, Michael, Keene, Kelly, Lin, Hui-Chuan, Michalakes, John, Rizvi, Syed, Zhang, Xin, Berner, Judith, & Smith, Kate. 2015. *WRF ARW Version 3 Modeling System User's Guide*. Mesoscale & Microscale Meteorology Division, National Centre for Atmospheric Research.
- Wu, Dong L., & Lee, Jae N. 2012. Arctic low cloud changes as observed by MISR and CALIOP: Implication for the enhanced autumnal warming and sea ice loss. *Journal of Geophysical Research: Atmospheres*, **117**(D7).